

Grinding heat flux distribution by an inverse heat transfer method with a foil/workpiece thermocouple under oil lubrication

Bruno Lavisse^{1,2} · André Lefebvre¹ · Olivier Sinot¹ · Emerik Henrion¹ · Samuel Lemarié² · Albert Tidu¹

Received: 27 October 2016 / Accepted: 20 February 2017 / Published online: 12 April 2017
© Springer-Verlag London 2017

Abstract In this paper, an inverse matching method with a foil/workpiece thermocouple is used to determine the global heat flux distribution and energy partition in the workpiece when grinding under oil lubrication. Low-pass filtering and sampling frequency of the temperature measurement in the inverse matching method are of particular importance, given fast variations of the heat flux at the wheel-workpiece interface. In the inverse method, low-pass filtering and sampling have a negligible influence on the average heat flux but not on the maximum heat flux. The mean heat flux in the region of positive heat flux and the partition ratio are determined under no-burn and burn grinding conditions. The new heat flux distribution estimated by a scalene triangle in the grinding zone and an exponential function in the convective cooling zone is in very good agreement with the test temperature profiles.

Keywords Grinding · Temperature · Thermocouple · Heat flux distribution

1 Introduction

Grinding is widely used in the industry for manufacturing components requiring a very precise surface finish. However, it requires a very high specific energy compared to other

conventional machining processes. Almost all of the energy is converted into heat in the grinding zone between the wheel and workpiece which causes a temperature rise. Therefore, an uncontrolled grinding process and high temperatures result in thermal damage to the workpiece (such as burnings, cracks, softening, or re-hardening of the surface layer) [1, 2]. It also accelerates the grinding wear, leading to a decrease of the grinding wheel performance [2]. Thus, research into the temperature generated in grinding is very important and many methods have been developed to measure the temperature in the contact zone [3, 4] and to determine the thermal balance under varying grinding conditions [5, 6]. The temperature measurement from an inverse method is used to identify the heat flux distribution in the grinding zone. [6] Parabolic, triangular, or uniform heat fluxes are commonly used to estimate the maximum background temperature provided that the partition coefficient is well known. However, this is not necessarily the case in wet grinding. Guo and Malkin [7, 8] studied three inverse heat transfer methods (temperature matching, integral, and sequential methods) with an embedded thermocouple to determine the heat flux distribution and convection heat transfer coefficient. Carvahlo et al. [9] proposed a more accurate solution by the conjugate gradient method of function estimation. Kim et al. [10] used a sequential method to determine the heat flux distribution in creep feed grinding, demonstrating that the scalene triangle model is better than the uniform and right-angled triangle models. The main drawbacks of these inverse methods with embedded thermocouple are as follows:

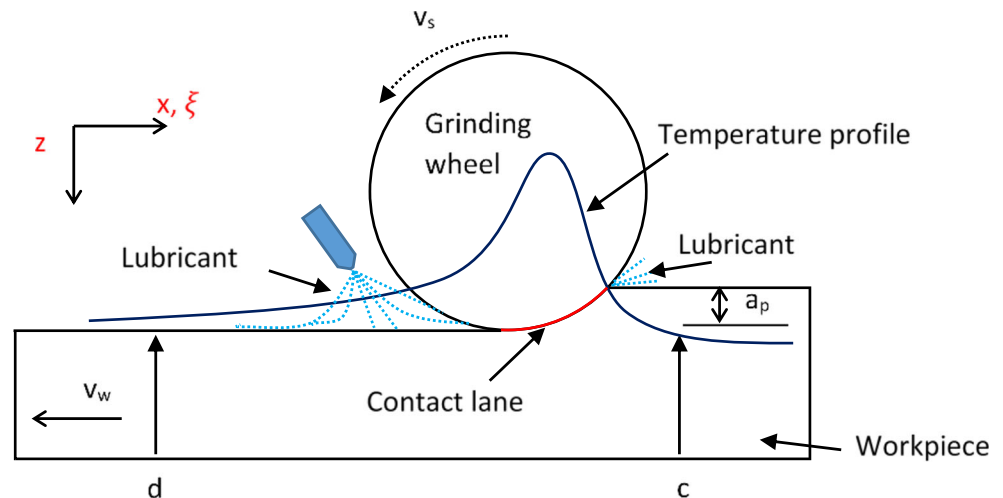
- Failure of the sequential method to estimate accurately the peak of the triangular heat flux distribution with simulated temperature measurements [9]
- Measurement uncertainty regarding the position of the junction in relation to the ground surface, which is often ignored in estimating the heat flux.

✉ André Lefebvre
andre.lefebvre@univ-lorraine.fr

¹ Laboratoire d'Étude des Microstructures et de Mécaniques des Matériaux (LEM3), CNRS UMR 7139, Université de Lorraine, Ecole Nationale d'Ingénieurs de Metz, 57078, Metz Cedex 03, France

² DCNS - Centre de Nantes-Indret, Nantes, France

Fig. 1 Grinding of a plane surface



- Higher measured temperature due to the disruption of the heat conduction around the thermocouple junction [11]
- A large number of temperature responses close to the ground surface are needed to approximate the temperature gradient by a finite difference and to determine the distance between ground surface and junction.

Recently, Pang et al. [12] proposed a Rayleigh curve heat flux distribution in cylindrical grinding that differs greatly from the typical triangular heat flux distribution in the grinding zone.

In this study, the heat flux distribution in a wet grinding (neat oil) inverse method is determined using a method developed by Guo and Malkin [7]. To apply this method, a single temperature signal is needed at a set depth below the ground surface. The temperature was measured with a single-pole foil/workpiece thermocouple, given the short time constant and measurement directly at the wheel-workpiece interface [13–15]. Before calculating the heat flux shape, the raw signal had to be filtered due to the many temperature flashes and electrical noise. The effect of filtering and sampling on the heat flux distribution was thus investigated, and an acceptable signal processing method was chosen. To get a heat flux distribution permits to determine the maximum and the mean of

the heat flux, the position of the maximum heat flux, as well as the partition ratio. Three heat source profiles were then tested using a set level of heat flux: right-angled triangular, scalene triangular, and scalene followed by exponential cooling. Those profiles were applied to estimate the workpiece temperature in the grinding zone and compared to test temperature measurements. Lastly, to determine the most consistent settings for the third heat flux model, temperatures predicted by the model were correlated to test temperature measurements.

2 Symbols and abbreviation

[C]		c_{ji} matrix
a_p	μm	Nominal depth of cut
a_{ed}	μm	Depth of dressing cut
b	m	Width of cut
C_p	$\text{J kg}^{-1} \text{K}^{-1}$	Specific heat capacity
D_{max}	%	$(l_{\text{max}}/l_g) \times 100$

Fig. 2 Heat flux discretization

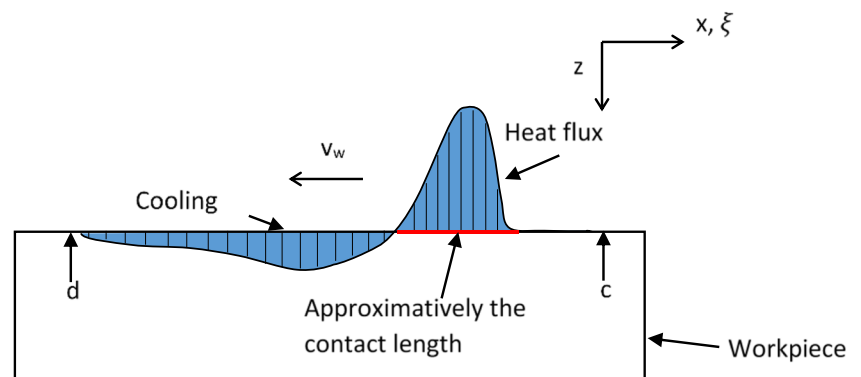


Table 1 Thermophysical properties of 32CrMoV12-9 between 0 and 300 °C

	32CrMoV12-9		
	0 °C	Average	300 °C
Thermal conductivity (W mK ⁻¹)	49	45	49
Thermal diffusivity (m ² s ⁻¹)	1.37 × 10 ⁻⁵	1.17 × 10 ⁻⁵	9.60 × 10 ⁻⁶
Density (kg m ⁻³)	7860	7790	7720
Specific heat capacity (J K ⁻¹ kg ⁻¹)	442	506	570

f	Hz	Frequency
f_{co}	Hz	Cutoff frequency
f_s	Hz	Sampling frequency
h_c	W m ⁻² K ⁻¹	Heat convection coefficient
K_0		Modified Bessel function second degree, order zero
l_c	m	Length of cooling domain
l_g	m	Geometric contact length
l_{hf}	m	Length of positive heat flux
l_{max}	m	Distance between maximum heat flux and cooling domain
l_r	m	Actual contact length
P_t	W	Grinding power
Q_w	W	Heat part conducted into the workpiece
$q_w(\xi)$	W m ⁻²	Heat flux distribution into the workpiece
q_c	W m ⁻²	Minimum of heat flux in the cooling part
q_{wm}	W m ⁻²	Mean heat flux
T_w	°C	Background temperature
U_d		Overlap ratio
V_s	m s ⁻¹	Wheel speed
V_{sd}	m s ⁻¹	Dressing wheel speed
V_w	m s ⁻¹	Workpiece speed
$\sqrt{(\lambda\rho C)_w}$	W s ^{-1/2} K ⁻¹ m ⁻²	Workpiece material thermal effusivity
α_w	m ² s ⁻¹	Workpiece material thermal diffusivity
λ_w	W m ⁻¹ K ⁻¹	Workpiece material thermal conductivity

ξ	m	Local coordinate in x -direction
ρ	kg m ⁻³	Mass density
β		Constant
τ_c	s	Time constant

3 Inverse method to deduce heat flux in grinding

Considering the workpiece a semi-infinite body and the moving heat flux theory [16], the quasi-steady-state temperature distribution between two coordinates (d and c) (Fig. 1) is given by Eq. 1 [7]

$$T_w(x, z) = \int_d^c \frac{q_w(\xi)}{\pi\lambda_w} \exp\left[-\frac{V_w(x-\xi)}{2\alpha_w}\right] K_0\left[\frac{V_w\sqrt{(x-\xi)^2 + z^2}}{2\alpha_w}\right] d\xi \quad (1)$$

Coordinates d and c correspond to the input/output domain. In Eq. 1, $q_w(\xi)$ is the local heat flux distribution on the top of the workpiece.

Table 2 Grinding parameters

Grinding parameters	
V_s (m s ⁻¹)	32
V_w (m s ⁻¹)	0.033
a_p (µm)	20–40–60
Flow rate (L min ⁻¹)	44
Wheel	Aluminum oxide Grit mesh size = 60 Average grain diameter = 253 µm
Dressing	Single point $U_d = 3$ $V_{sd} = 32$ m s ⁻¹ $a_{ed} = 10$ µm

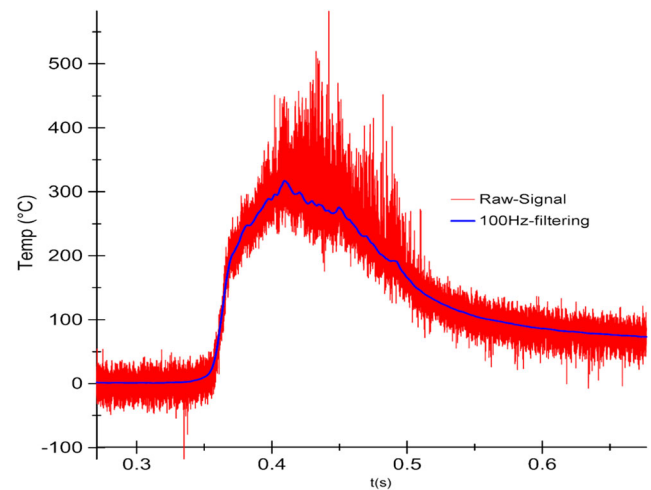


Fig. 3 Raw signal vs. filtered signal with $f_{co} = 100$ Hz ($a_p = 60$ µm, $V_w = 0.033$ m s⁻¹, $V_s = 32$ m s⁻¹, oil lubricant)

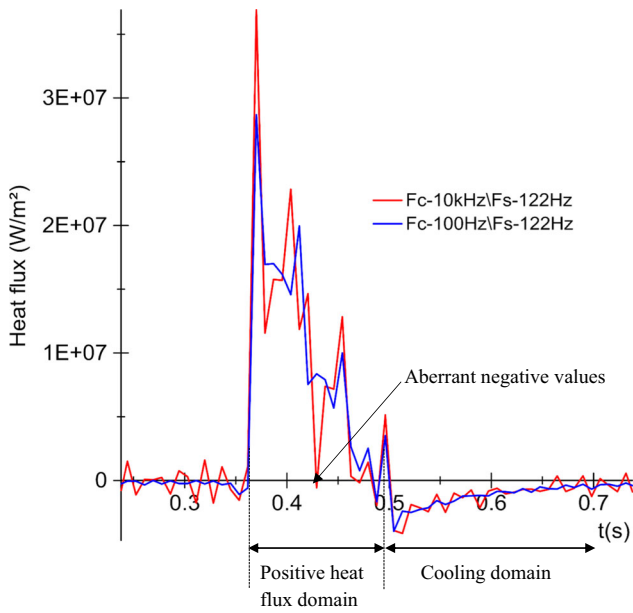


Fig. 4 Heat flux after 10 kHz vs. 100 Hz low-pass filtering ($f_s = 122$ Hz)

The heat flux distribution on the segment $[d, c]$ is divided into n equal segments in each of which the heat flux is approximated by constant q_i . The steady-state temperature distribution is given by Eq. 2 [7] (Fig. 2)

$$T_w(x, z) = \sum_{i=1}^n \frac{q_i}{\pi \lambda_w} \int_{\xi_i}^{\xi_{i+1}} \exp\left[-\frac{V_w(x-\xi)}{2\alpha_w}\right] K_0 \left[\frac{V_w \sqrt{(x-\xi)^2 + z^2}}{2\alpha_w} \right] d\xi \tag{2}$$

Using n test temperature points in the sum in Eq. 2 and considering n equally spaced points, x_j ($j = 1, 2, \dots, n$), an n -simultaneous system of n unknowns is obtained [7]

$$T_j = \sum_{i=1}^n c_{ji} q_i \text{ with } j = 1, 2, \dots, n \tag{3}$$

where c_{ji} is expressed by [7]

$$c_{ji} = \int_{\xi_i}^{\xi_{i+1}} \frac{1}{\pi \lambda_w} \exp\left[-\frac{V_w(x_j-\xi)}{2\alpha_w}\right] K_0 \left[\frac{V_w \sqrt{(x_j-\xi)^2 + z^2}}{2\alpha_w} \right] d\xi \quad (j = 1, 2, \dots, n) \tag{4}$$

Once such grinding parameters as depth of cut, workpiece speed, grinding wheel speed, and thermophysical properties are set, matrix $[C]$ may be calculated. The n discrete heat fluxes, $\{q\} = \{q_1, q_2, \dots, q_n\}$, are obtained by matrix inversion (Eq. 5), and n equally spaced temperature measurements,

$\{T\} = \{T_1, T_2, \dots, T_n\}$, are expressed as follows [7]:

$$\{q\} = [C]^{-1} \{T\} \tag{5}$$

where $[C]$ is the matrix composed of the term c_{ji} .

With this method, a heat flux distribution with a single temperature measurement at a given depth (z) can be used.

3.1 Test setup and grinding parameters

The workpiece material is 32CrMoV12-9 alloy steel. A foil/workpiece thermocouple consisting of a Constantan foil insulated by two mica sheets is inserted between two parts of the 32CrMoV12-9 steel block [14, 17, 18]. Since one electrode is the workpiece and the other the Constantan foil, it is called an “intrinsic thermocouple.” The Constantan foil is 25 μm thick and 2 mm wide. The thermocouple output voltage is amplified by a signal conditioning extension (SCXI-1100) with cold junction compensation and sampled at 1.25 MHz by a NI 6071-E data acquisition device [19]. The high sampling rate allows us to monitor the stability and the quality of the junction during grinding. Lefebvre et al. [19] showed that the maximum background temperature to be measured can thus be estimated, but roughly due to the uncertainty in the normal heat flux at the junction after grinding by grits. In this study, the contact time between the thermocouple junction and the wheel is long (>50 ms) and the work speed is slow (<50 mm s^{-1}). Consequently, the transparency error of the sensor on the maximum background temperature is estimated (with a finite element model) to be about 5%. The time constant of the foil/workpiece thermocouple is a few milliseconds for longitudinal loading, whereas the

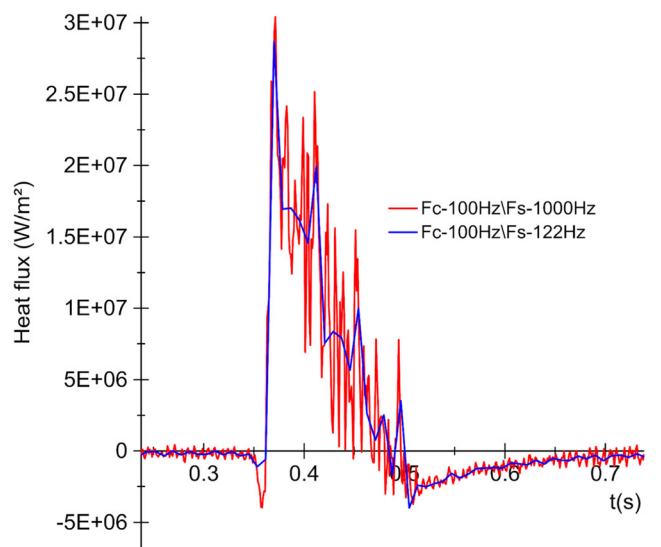


Fig. 5 Heat flux with 1000 Hz vs. 122 Hz sampling frequency ($f_{co} = 100$ Hz)

Table 3 Average and maximum heat flux vs. low-pass filtering frequency ($f_s = 122$ Hz)

	Filter frequency							Raw	Average	Standard deviation
	100	500	1000	5000	10,000	50,000	100,000			
Average heat flux ($W\ mm^{-2}$)	8.15	8.14	8.13	8.23	8.23	8.31	8.39	8.01	8.20	0.11
Maximum heat flux ($W\ mm^{-2}$)	28.7	31.7	33.1	36.3	36.9	36.4	37.4	39.9	35.05	3.6

time constant associated with local junction heating by active grits is only a few microseconds [14, 19]. Since the minimum contact time is 85 ms in this study, the error due to longitudinal thermal inertia can be ignored.

For the inverse method, the z -coordinate was set to 1 μm since the junction is just below the wheel-workpiece-lubricant interface. A realistic order of magnitude for junction thickness based on actual chip thickness and surface roughness is about 1 μm .

The thermophysical properties of the material are given in Table 1.

To take into account the variation in thermal properties with temperature, an average between 0 and 300 $^{\circ}C$ was used to minimize the error on the heat flux.

In this study, grinding parameters that were kept constant include workpiece speed ($V_w = 0.033\ m\ s^{-1}$) and wheel speed ($V_s = 32\ m\ s^{-1}$). Table 2 shows the grinding parameters. In this table, the grain size is determined by the size of mesh of a sieve through which the grain can pass.

For the tests, the lubricant flow rate was 44 $L\ min^{-1}$ with a jet speed of 11 $m\ s^{-1}$.

3.2 Effect of temperature filtering on heat flux distribution

The temperature signal has two components: temperature flashes due to the grinding grits and a background temperature [14] (Fig. 3). The background temperature is that of interest for thermal damage to the workpiece. The composite signal must thus be filtered (generally with a low-pass filter) to remove the temperature flashes. Since earlier studies found that the temperature distribution is very sensitive to filter parameters and the heat flux may depend slightly on those chosen, a

preliminary study was conducted on the effect of filtering on the heat flux distribution.

Figure 3 shows the temperature distribution after low-pass filtering with a cutoff frequency (f_{co}) = 100 Hz. The resulting signal closely approximates the background temperature. The cutoff frequency was thus set to 100 Hz for the study. The most appropriate filter parameters had to be chosen to determine the influence of the filtered temperature on the heat flux shape.

In an investigation by Zhu et al. [20], temperatures measured in the workpiece subsurface were found to be consistent with a triangular heat flux (close to a triangular shape over approximately the contact length) followed by a negative heat flux area corresponding to a cooling zone. The most appropriate filter parameters are thus the ones resulting in a heat flux distribution with two distinct, well-separated domains.

Figure 4 shows the heat fluxes after filtering with $f_{co} = 10\ kHz$ and $f_{co} = 100\ Hz$ and with a sampling frequency (f_s) = 122 Hz. As observed in Fig. 4, the heat flux obtained with $f_{co} = 10\ kHz$ has aberrant values, several negative values in the middle part of the contact length, and a poorly defined cooling part. On the other hand, the filtered signal with $f_{co} = 100\ Hz$ has a positive heat flux domain nearly triangular in shape and a more distinct cooling part.

The influence of filtering on the average positive heat flux also required a study. To determine the energy partition to the workpiece, the average heat flux (q_{wm}) conducted into the workpiece is needed. It is thus crucial to know whether filtering parameters (i.e., cutoff and sampling frequencies) affect the average heat flux and the heat flux distribution at the wheel-workpiece interface.

Table 4 Average and maximum heat flux vs. sampling frequency ($f_{co} = 100$ Hz)

	Sampling frequency			Average	Standard deviation
	122	1000	3054		
Average heat Flux ($W\ mm^{-2}$)	8.15	8.64	8.6	8.47	0.25
Maximum heat Flux ($W\ mm^{-2}$)	28.7	30.4	31.7	30.22	1.5

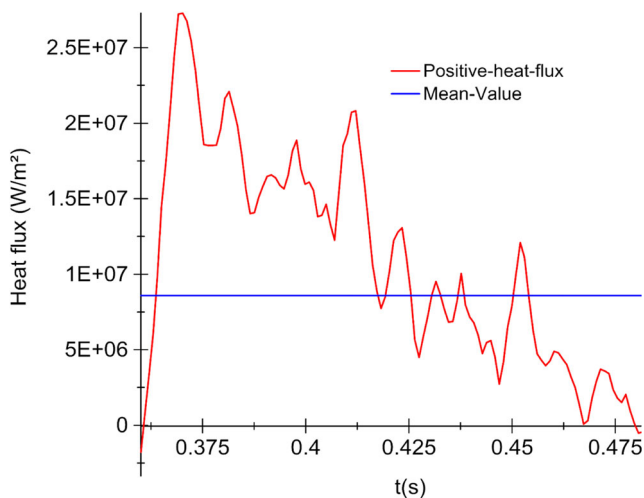


Fig. 6 Average heat flux in the grinding zone ($f_{co} = 100$ Hz and $f_s = 1$ kHz)

Figure 5 shows the heat flux distribution for $f_s = 1000$ Hz and $f_s = 122$ Hz, with $f_{co} = 100$ Hz.

Sampling at 122 Hz gave a smoother heat flux shape; however, it gives about 15 points in the contact length. Using a 1000 Hz sampling (about hundreds of heat fluxes, q_i) enables to obtain a better heat flux resolution.

To complete the preliminary study on filtering, eight low-pass filters were tested with $f_s = 122$ Hz. It can be concluded from the results that the average heat flux obtained by the inverse method is independent of the cutoff frequency (Table 3). A too low sampling frequency tends to result in a slightly underestimated average heat flux, while higher ones do not give more precise results but considerably increase computation time (Table 4).

All tests presented below thus use 100-Hz low-pass filtering and a sampling frequency of 1000 Hz. Since Tables 2 and 3 reveal that the maximum heat flux is

sensitive to signal processing, however, only the average heat flux was considered in this study.

4 Heat partition ratio and heat flux distribution under an oil lubricant

The heat partition ratio (R_w) in grinding has been investigated in many studies [1, 4, 18, 20]. It is widely acknowledged that the overall grinding power is divided between the workpiece, grinding wheel, lubricant, and chips. Lavine et al. [21] show that relatively little energy is dissipated into the chips. Grinding energy is thus mainly divided into the grinding wheel, workpiece, and lubricant.

The partition coefficient (R_w) is defined by the following expression:

$$R_w = \frac{Q_w}{P_t} \quad (6)$$

where $P_t = F_t V_s$ with F_t as the tangential grinding force and V_s as the wheel velocity.

By using this coefficient, a good approximation of the maximal temperature rise (T_{maxi}) in the grinding zone can be obtained with the tangential force (or power measurement)

$$T_{maxi} = \beta \frac{R_w F_t V_s}{b \sqrt{l_g} \sqrt{(\lambda \rho C)_w V_w}} \quad (7)$$

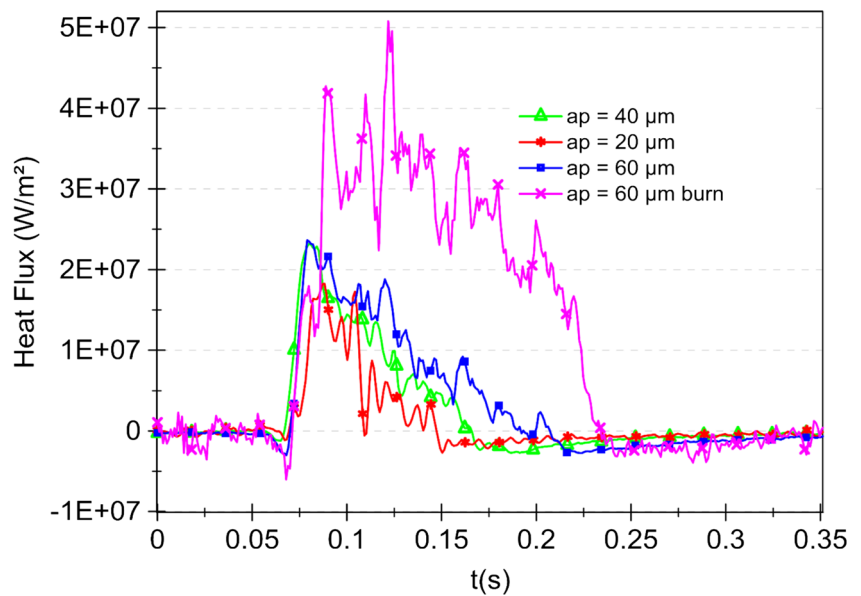
where β is equal to 1.13, 1.06, and 1.2 for uniform, triangular, and square heat flux distributions, respectively.

The inverted heat flux distribution (Fig. 5) is calculated from the temperature distribution.

Table 5 R_w for different grinding conditions

Burning	a_p (μm)	F_t (N mm^{-1})	q_{wm} (W mm^{-2})	V_s (m s^{-1})	T_{wmax} ($^{\circ}\text{C}$)	l_g (mm)	R_w (-)
No	20	1.38 ± 0.1	6.16	32	169	2.8	0.40 ± 0.02
No	20	1.44 ± 0.1	6.27	32	174	2.8	0.40 ± 0.02
No	40	2.90 ± 0.1	10.6	32	290	3.3	0.38 ± 0.02
No	40	2.54 ± 0.1	8.95	32	250	3.3	0.39 ± 0.01
No	60	3.55 ± 0.2	8.80	32	299	4.8	0.41 ± 0.02
Yes	60	6.75 ± 0.7	25.9	32	792	4.8	0.62 ± 0.06
Yes	60	6.15 ± 0.7	22.9	32	792	4.8	0.69 ± 0.07
Yes	60	6 ± 0.7	23.7	32	804	4.8	0.65 ± 0.08
Yes	60	6 ± 0.7	22.1	32	771	4.8	0.69 ± 0.08

Fig. 7 Heat flux distribution for different depths of cut



4.1 Mean heat flux and partition ratio

The average heat flux is obtained by integration of the positive part of the heat flux distribution (Fig. 6). As mentioned earlier, this positive part roughly corresponds to the contact length.

Average grinding forces were measured using a Kistler dynamometer. To be certain to acquire only net grinding forces, fluid forces were subtracted from the total forces by recording the forces in a spark-out pass with zero depth of cut. An average heat transfer coefficient (R_w) is then obtained from Eq. 6.

4.2 Test results

For the five first passes, an initial dressing was made. For the last four rows of Table 5, there was no dressing and burn thus occurs.

The partition ratio (R_w) is clearly higher for burning passes, rising from about 0.4 for passes with no burn to about 0.66 for passes with thermal damage. This increase of about 65% can be explained by the rise in background temperature to a maximum of about 800 °C, higher than the boiling point of the lubricating fluid (300 °C), which thus lost its efficiency.

Fig. 8 Heat flux distribution with a 4-ms running average filter

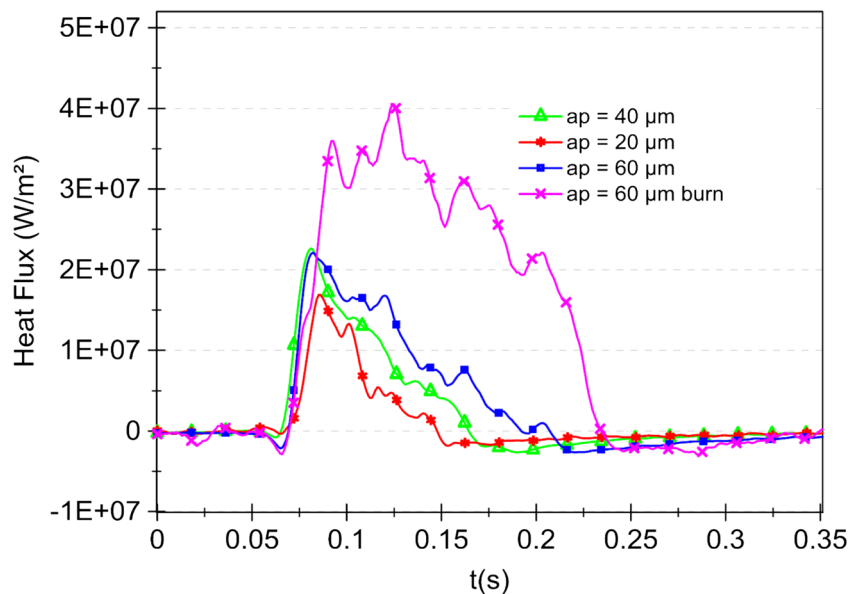


Fig. 9 Heat flux distribution with 100-Hz low-pass filtering ($f_s = 1$ kHz) compared to the temperature distribution with 1 kHz low-pass filtering

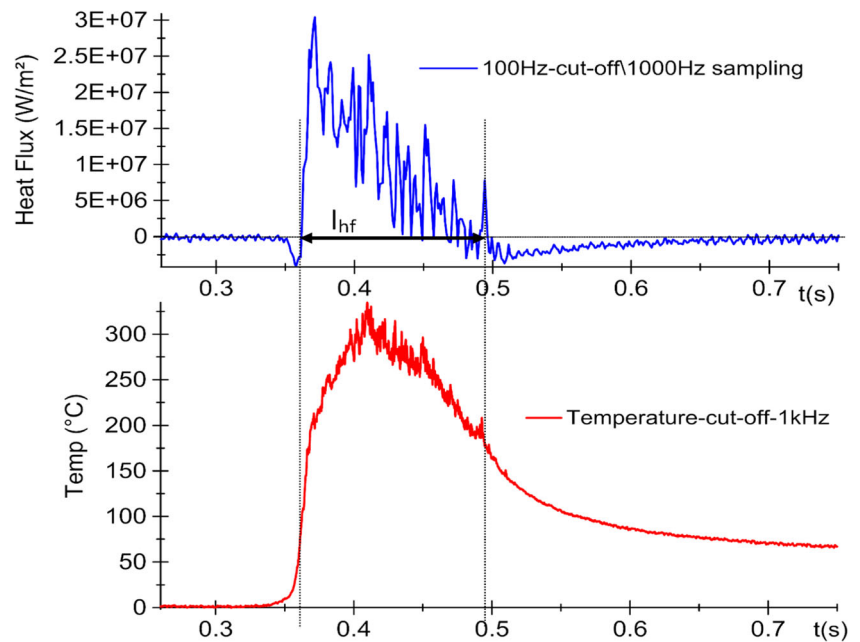


Figure 7 presents several heat fluxes obtained by the inverse method described earlier. In the cooling part, the minimum heat flux is similar in all tests. It can also be seen that burning leads to increased depth of cut. The positive heat flux part is clearly longer for “ $a_p = 60 \mu\text{m}$ burn” than for “ $a_p = 60 \mu\text{m}$.” This can be explained by thermal expansion of the workpiece due to the high temperature in the grinding zone (800°C).

The heat flux distribution in Fig. 7 appears approximately triangular in shape. The variation in the test heat flux is due to the small variation in background temperature after 100-Hz low-pass filtering, as seen in Fig. 3. Adding a 4-ms running average filter results in a more triangular heat flux shape (see Fig. 8). The position of the maximum heat flux is thus clearly identified without significantly changing its position and value.

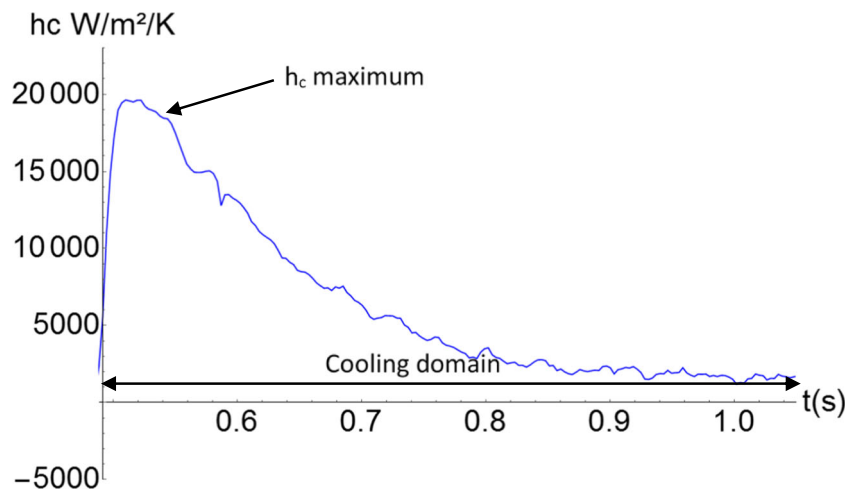
4.3 Positive heat flux length and position of the maximum heat flux

In Fig. 9, the temperature distribution is on the same scale as the heat flux. The length of the positive heat flux (l_{hf}) is represented. It appears that l_{hf} is slightly shorter than the real contact length (temperature spikes are following the end of l_{hf}). It is in accordance with Rowe et al. [22] who shows that the real contact length is longer than the geometrical contact length. At the end of the contact, the number of the active grits is decreasing and the local heat flux conducted to the workpiece from the active grits is not sufficient to compensate the cooling due to the lubricant. That is why the real contact length defined by temperature spikes is longer than the length of positive heat flux.

Table 6 Contact length, positive heat flux length, maximum heat flux position, and minimum heat flux convective coefficient for different depths of cut

Burning	a_p (μm)	l_g (mm)	l_{hf} (mm)	d_{max} (%)	h_{cmax} ($\text{kW m}^{-2} \text{K}^{-1}$)
No	20	2.79	2.61	69.2	24.7
No	20	2.79	2.69	69.8	26.2
No	40	3.33	3.25	81.1	29.4
No	40	3.33	3.29	83.2	30.2
No	60	4.83	4.65	80.6	17.8
Yes	60	4.83	5.30	76.0	4.1
Yes	60	4.83	6.00	75.6	4.0

Fig. 10 Heat convective coefficient in the cooling part for grinding conditions $a_p = 60 \mu\text{m}$, $V_w = 0.033 \text{ m s}^{-1}$, $V_s = 32 \text{ m s}^{-1}$, and oil lubricant at 40 L min^{-1}



In Table 6, the geometric contact length (l_g) and the length of positive heat flux (l_{hf}) are compared. For tests without burn, l_{hf} is less than 10% shorter than l_g . These results show that with these grinding conditions, the approximation of the heat source length by the geometric contact length was a good fit.

The position of maximum heat flux on the contact length was also investigated. This position is determined based on the distance between the maximum heat flux and the position where the heat flux become negative. It is expressed as a percentage of l_g . The maximum heat flux falls between 69.2 and 83.2% for tests with no burn and between 76 and 87% for tests with burn. The position of the maximum heat flux is more difficult to determine for tests with burn. Later in the study, an average d_{max} of 75% ($\pm 6\%$) is used for modeling tests with no burn.

4.4 Cooling region

The cooling heat flux in the grinding zone is often modeled by a constant convection heat transfer coefficient (CHTC) outside the grinding zone. Based on the finite difference method

and embedded thermocouple measurements, Shen et al. [23] proposed, in addition to the triangular heat flux distribution, a linearly varying CHTC in the grinding zone. Using the present method, heat flux convective coefficient (h_c) is calculated for each grinding pass in the cooling domain. Table 5, with the same grinding parameters as in Table 4, shows that the maximum h_c is roughly $20 \text{ kW m}^{-2} \text{ K}^{-1}$, consistent with values in the literature.

However, this coefficient is often taken as constant. In Fig. 10, h_c first peaks and then tapers off toward zero. The average h_c would thus be an inaccurate approximation. The goal of this study is to propose a model that takes this h_c profile into account and fit the cooling part, given the oil lubricant.

The cooling part was obtained by fitting an exponential function (Eq 8) as shown in Fig. 11

$$q_{cooling}(x) = -q_c e^{-\left(\frac{x-(l_c-d_1)}{V_w \tau_c}\right)} \tag{8}$$

where τ is the time constant and d_1 is the position of the maximum convective heat flux

Fig. 11 Fitting of the heat flux cooling part for a grinding test with $a_p = 60 \mu\text{m}$, $V_w = 0.033 \text{ m s}^{-1}$, $V_s = 32 \text{ m s}^{-1}$, filtering cutoff frequency = 100 Hz, and oil lubricant = 40 L min^{-1}

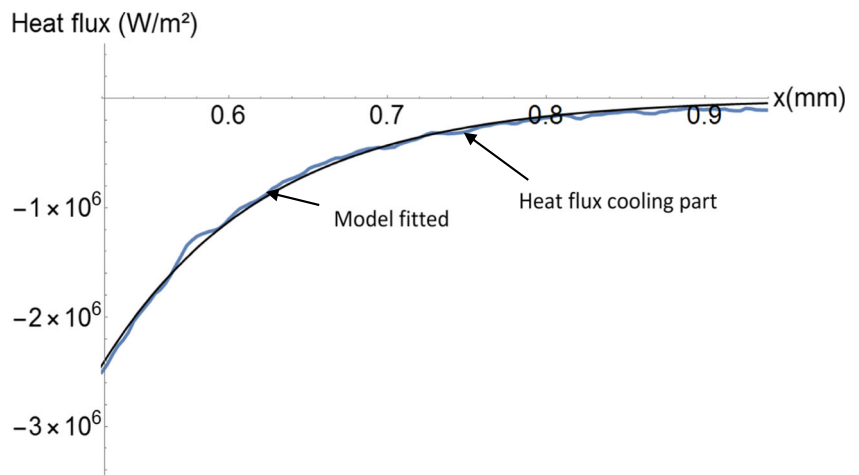


Table 7 Values of q_c and τ_c for tests with no burn

Burning	a_p (μm)	q_c (MW m^{-2})	τ_c (s)
No	20	2.0	0.08
No	20	2.1	0.09
No	40	2.6	0.08
No	40	3.0	0.07
No	60	2.7	0.10

$$d_1 = \frac{q_c l_{\text{max}}}{2q_w} \tag{9}$$

For each test, the best value of q_c and τ was obtained by a least-squares refinement and is shown in Table 7.

5 Validation of the heat flux distribution model

In this section, it is shown that with a model heat flux, reliable partition ratio (R_w), tangential force measurement, and mean values of maximum cooling heat flux (q_c) and cooling time constant (τ_c), the temperature distribution for 32CrMoV12-9 steel under oil lubrication can be estimated.

5.1 Heat flux models

To validate the heat flux model obtained with the inverse method, the quasi-steady-state numerical temperature (obtained using the analytical solution of the moving heat source) is compared to the test temperature.

Three heat flux distributions ($q_w(x)$) are tested to determine the temperature profile:

- Right-angled triangle (rat) heat flux without convective cooling, $q_{w\text{-rat}}(x)$
- Scalene triangle heat flux (sct) without convective cooling, $q_{w\text{-sct}}(x)$
- Scalene triangle heat flux with exponential convective cooling (sct-conv), $q_{w\text{-sct-conv}}(x)$

In Table 8, the first and second distributions are respectively the right-angled triangle and scalene triangle heat fluxes tested and their respective equations. Note that those two types of heat flux ignore the cooling domain. The third row of Table 6 presents the scalene heat flux distribution with convective cooling.

Models are matched using the mean heat flux (q_{wm}) defined as

$$q_{wm} = R_w \frac{F_t V_s}{b l_g}$$

Table 8 The different heat flux distributions and their representative function

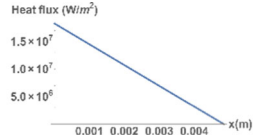
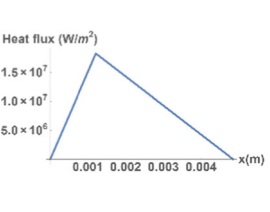
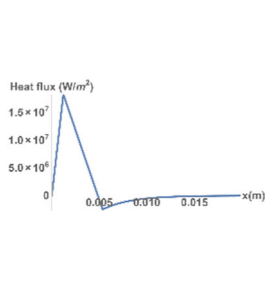
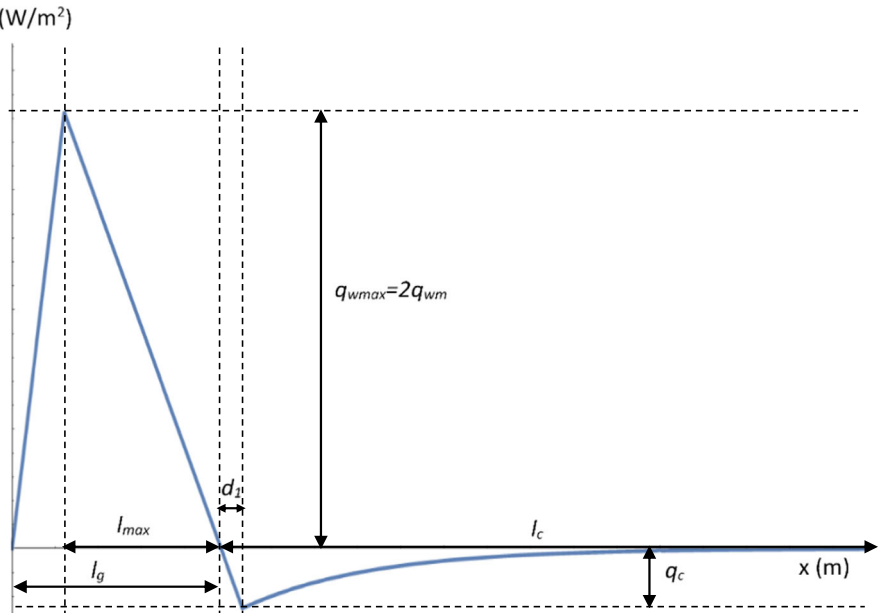
	$q_{w\text{-rat}}(x) = 2q_w \frac{l_g - x}{l_r}$ <p style="text-align: center;">Eq 1</p>
	$q_{w\text{-sct}}(x) = \begin{cases} 2 \frac{q_{wm} x}{l_e - l_{max}}, & 0 \leq x \leq l_g - l_{max} \\ 2 \frac{q_{wm} (l_g - x)}{l_{max}}, & l_g - l_{max} \leq x \leq l_g \end{cases}$ <p style="text-align: center;">Eq 2</p>
	$q_{w\text{-sct-conv}}(x) = \begin{cases} 2q_{wm} \frac{x}{l_g - l_{max}} & 0 \leq x \leq l_g - l_{max} \\ 2q_{wm} \frac{(l_g - x)}{l_{max}} & l_g - l_{max} \leq x \leq l_g + d_1 \\ -q_c e^{-\frac{x - (l_g - d_1)}{V_w \tau}} & l_g + d_1 \leq x \leq l_g + l_c \end{cases}$ <p style="text-align: center;">Eq 3</p>

Fig. 12 Heat flux model diagram



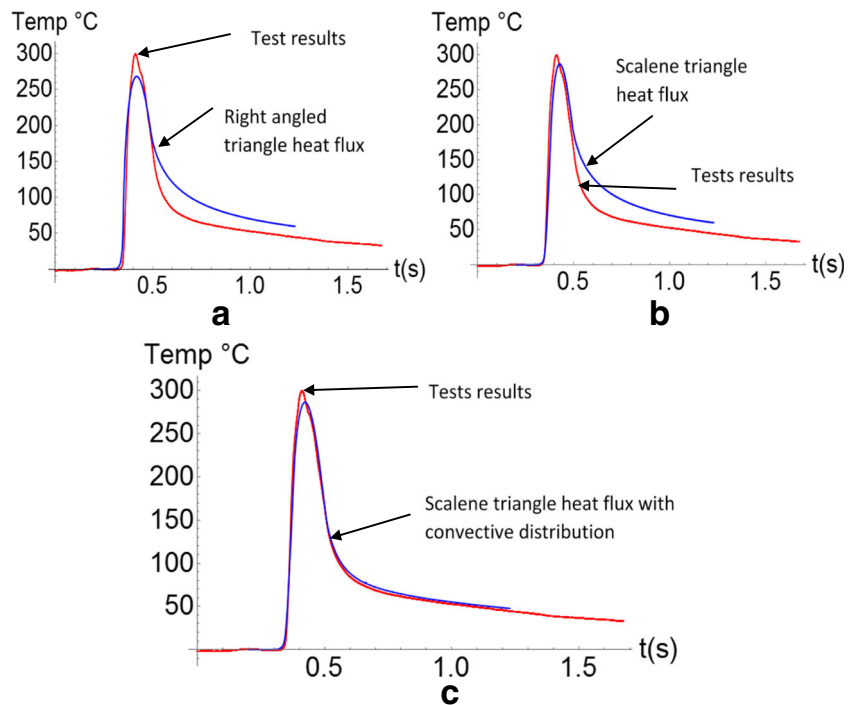
where F_t is the tangential force, bl_g is the geometric wheel-workpiece contact surface, and R_w is the partition ratio, equal to 0.4 and identical for the tests with no burn.

This mean heat flux density (q_{wm}) is the same for all three models.

The position of the maximum heat flux in the scalene distribution (Table 8, row 2) was determined by applying the inverse heat transfer analysis previously described to the test

results, taking the average d_{max} of all tests. As explained earlier, $d_{max} = 75\%$ is taken for $l_{max} = 3.62$ mm. Results are presented in Fig. 13a–c). Figure 9 and Table 8 show that q_c is apparently the same for the various test heat fluxes. An average q_c of 2.5 MW m^{-2} and constant cooling time (τ) of 0.88 s are thus taken to determine the convective heat flux function, $q_{cooling}(x)$. The position of the maximum heat flux is the same as in the simple scalene triangle distribution

Fig. 13 Test results compared to temperatures estimated by a heat flux model of type. **a** Right-angled triangle. **b** Scalene triangle. **c** Scalene triangle with convective cooling



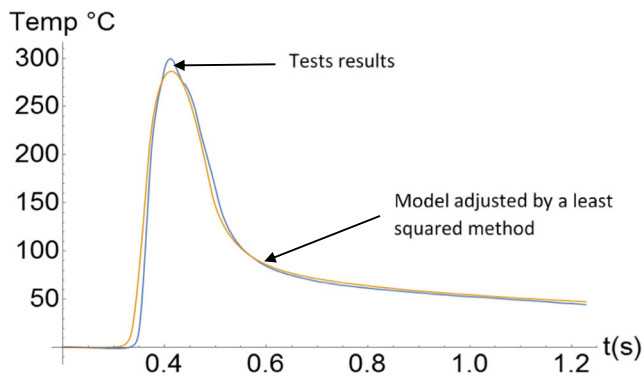


Fig. 14 Model adjusting on abscissa axis

(Table 6, row 2). The resulting model is represented in Table 8, row 3.

To clarify, all values in Table 8 are shown in Fig. 12.

5.2 Comparison between test temperature measurements and model estimates

Using the right-angled triangular heat flux, the maximum temperature is underestimated by about 30 °C. The cooling part is much higher, however, than on the test curve (Fig. 13a). The scalene triangle heat flux provides a slightly better maximum temperature estimate, but the cooling part is still much higher than the test curve (Fig. 13b). Lastly, the workpiece temperature estimated using a scalene triangle with convective cooling fits the test temperature profile very closely along the temperature rise, at the peak and along the cooling phase (Fig. 13c).

A major source of error in the correlation is uncertainty associated with the origin of the two curves (model and tests) on the X -axis. To correct this problem, the position of the analytical heat source is adjusted along the time axis using a least-squares method (Fig. 14).

Table 9 summarizes the correlation between model estimates and test measurements for tests with no burn. The

Table 9 Correlation between model and temperature measurements for tests with no burn ($V_w = 0.033 \text{ m s}^{-1}$, $V_s = 32 \text{ m s}^{-1}$, 100-Hz low-pass filtering, and oil lubricant at 40 L min^{-1})

Burning	a_p (μm)	R^2	Δ_{max} ($^{\circ}\text{C}$)
No	20	0.993	13.2
No	20	0.994	17.2
No	40	0.997	20.5
No	40	0.997	33.9
No	40	0.994	20.2
No	60	0.998	26.9

correlation coefficient always exceeds 0.99 with a maximum difference of about 25 °C. The results prove that this type of heat flux shape provides suitable temperature estimates. It may thus be concluded that the scalene triangle heat flux followed by a decreasing exponential function to model convective cooling can be used to predict the temperature distribution in grinding 32CrMoV12-9 steel under an oil lubricant.

5.3 Flowchart of heat flux modeling and validation

The flowchart (Fig. 15) sums up the heat flux modeling methodology and its validation.

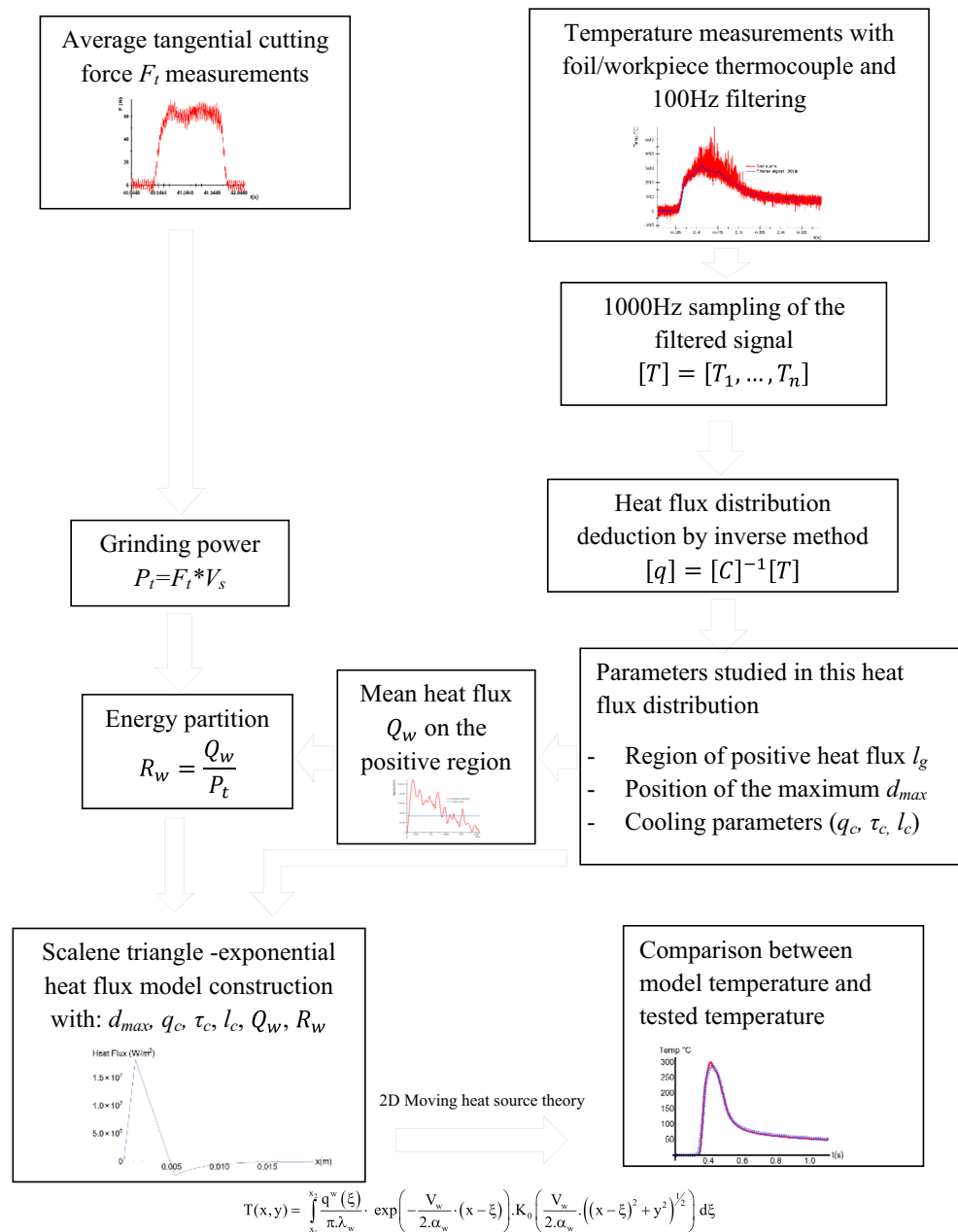
6 Conclusion and remarks

This work shows that in grinding, the use of an inverse method to determine the heat flux distribution with a foil/workpiece thermocouple is achievable and gives consistent results.

- Temperature measurements must be filtered before using them in the inverse method. This filtering affects the shape of the heat flux obtained, but the average heat flux derived from the inverse method is independent of the cutoff frequency.
- The inverse method combined with the test setup results in a partition coefficient R_w equal to 0.4 for tests with no burn and 0.65 for tests with burn, proving that the lubricant is effective directly at the wheel-workpiece interface when the temperature is lower than the lubricant's boiling point.
- The method also yields results fitting test variations in the heat transfer coefficient in the convective cooling domain
- The scalene triangle model with exponential cooling best fits test temperature results.

This study has shown that this type of heat flux model can be used to predict accurately the temperature distribution in the grinding zone of 32CrMoV12-9 steel under lubrication. Values of q_{wm} , q_c , τ_c , d_{max} , and R_w obtained with the inverse matching method from the foil/workpiece thermocouple may change depending on the workpiece material and grinding conditions. However, the entire methodology could perfectly well be used under other grinding conditions to evaluate the effectiveness of the grinding process and the onset of the grinding burn. The method also makes it possible to reliably predict the temperature distribution during grinding without any temperature sensors by measuring grinding power for industrial environments.

Fig. 15 Heat flux modeling its validation



References

1. A. Bell, T. Jin et D. J. Stephenson, Burn threshold prediction for high efficiency deep grinding, Int J Mach Tools Manuf, vol. 51, pp. 433–438, 2013.
2. B. Weiss, A. Lefebvre, O. Sinot, M. Marquer et A. Tidu, Effect of grinding on the sub-surface and surface of electrodeposited chromium and steel substrate, Surf Coat Technol, vol. 272, pp. 165–175, 2015.
3. X. Chen, W. B. Rowe et D. F. McCormack, Analysis of the transitional temperature for tensile residual stress in grinding, J Mater Process Technol, 107, (1–3), 216–221, 2000.
4. D. Anderson, A. Warkentin et R. Bauer, Comparison of numerically and analytically predicted contact temperatures in shallow and deep dry grinding with infrared measurements, Int J Mach Tools Manuf, 48, (3–4), 320–328, 2008.
5. E. Garcia, D. Méresse, I. Pombo, S. Harmand et J. A. Sanchez, Identification of heat partition in grinding related to process parameters, using the inverse heat flux conduction model., Appl Therm Eng, 66, (1–2), 122–130, 2014.
6. A. M. Tahvilian, Z. Liu, H. Champliand et B. Hazel, Experimental and finite element analysis of temperature and energy partition to the workpiece while grinding with a flexible robot, J Mater Process Technol, 213, 12, pp. 2292–2303, 2013.
7. C. Guo et S. Malkin, Inverse heat transfer analysis of grinding part 1: methods, Journal Engineering of Industry, vol. 118, pp. 137–142, 1996a.
8. C. Guo et S. Malkin, Inverse heat transfer analysis of grinding part 2: applications, Journal Engineering of industry, vol. 118, pp. 143–149, 1996b.

9. R. N. Carvahlo, H. R. Orlande et M. N. Özisik (2016) Estimation of the boundary heat flux in grinding via the conjugate gradient method 7632
10. H. Kim, N. Kim et J. Kwak, Heat flux distribution model by sequential algorithm of inverse heat transfer for determining workpiece temperature in creep feed grinding, *International Journal of Machine Tools & Manufacture*, vol. 46, pp. 2086–2093, 2006.
11. T. Obikawa, H. Takahara et T. Shirakahi, Energy flowing rate into workpiece in surface grinding based on 3, *International Journal of the Japan Society for Precision Engineering*, vol. 32, 1, pp. 19–24, 1998.
12. J. Pang, B. Li, Y. Liu et C. Wu (2016) Rayleigh heat flux distribution model investigation and workpiece temperature prediction in the cylindrical grinding. *Int J Adv Manuf Technol* 1–11
13. A. D. Batako, W. B. Rowe et M. N. Morgan, Temperature measurement in high efficiency deep grinding, *Int J Mach Tools Manuf*, vol. 45, pp. 1231–1245, 2005.
14. A. Lefebvre, F. Lanzetta, P. Lipinski et A. A. Torrance, Measurement of grinding temperatures using a foil/workpiece thermocouple, *Int J Mach Tools Manuf*, vol. 58, pp. 1–10, 2012.
15. D. Babic, D. B. Murray et A. A. Torrance, Mist jet cooling of grinding processes, *Int J Mach Tools Manuf*, vol. 45, 10, pp. 1171–1177, 2005.
16. Jaeger J (1942) Moving sources of heat and the temperature at sliding contacts. *Proceedings of the Royal Society of NSW* 76: 203–224
17. X. Xu et S. Malkin, Comparison of methods to measure grinding temperatures, *J Manuf Sci Eng*, vol. 123, pp. 191–195, 2001.
18. W. Rowe, S. Black, B. Mills, H. S. Qi et M. N. Morgan, Experimental investigation of heat transfer in grinding, *CIRP Ann Manuf Technol*, vol. 44, 329–332, 1995.
19. A. Lefebvre, P. Vieville, P. Lipinski et C. Lescalier, Numerical analysis of grinding temperature measurement by the foil/workpiece thermocouple method, *International Journal of Machine Tools & Manufacture*, vol. 46, pp. 1716–1726, 2006.
20. B. Zhu, C. Guo et J. Sunderland, Energy partition to the workpiece for grinding of ceramics, *Annals of the CIRP*, pp. 267–271, 1995.
21. A. Lavine, S. Malkin et T. Jen, Thermal aspects of grinding with CBN wheels, *CIRP Ann Manuf Technol*, vol. 38, pp. 557–560, 1989.
22. W. Rowe, M. Morgan, H. Qi et H. Zheng, The effect of deformation on the contact area in grinding, *CIRP Ann Manuf Technol*, vol. 42, pp. 409–412, 1993.
23. B. Shen, A. J. Shih et G. Xiao, A heat transfer model based on finite difference method for grinding, *J Manuf Sci Eng*, vol. 133, 3, pp. 1–11, 2011.